Chapter 5 The Ambiguity Function - Analog Waveforms

5.1. Introduction

The radar ambiguity function represents the output of the matched filter, and it describes the interference caused by the range and/or Doppler shift of a target when compared to a reference target of equal RCS. The ambiguity function evaluated at $(\tau, f_d) = (0, 0)$ is equal to the matched filter output that is perfectly matched to the signal reflected from the target of interest. In other words, returns from the nominal target are located at the origin of the ambiguity function. Thus, the ambiguity function at nonzero τ and f_d represents returns from some range and Doppler different from those for the nominal target.

The formula for the output of the matched filter was derived in Chapter 4, it is, assuming a moving target with Doppler frequency f_d,

$$\chi(\tau, f_d) = \int_{-\infty}^{\infty} \tilde{x}(t)\tilde{x}^*(t-\tau)e^{j2\pi f_d t}dt \tag{5.1}$$

The modulus square of Eq. (5.1) is referred to as the ambiguity function. That is,

$$\left|\chi(\tau, f_d)\right|^2 = \left|\int_{-\infty}^{\infty} \tilde{x}(t)\tilde{x}^*(t-\tau)e^{j2\pi f_d t}dt\right|^2 \tag{5.2}$$

The radar ambiguity function is normally used by radar designers as a means of studying different waveforms. It can provide insight about how different radar waveforms may be suitable for the various radar applications. It is also used to determine the range and Doppler resolutions for a specific radar waveform. The three-dimensional (3-D) plot of the ambiguity function versus frequency and time delay is called the radar ambiguity diagram.

Denote E_x as the energy of the signal $\tilde{x}(t)$,

$$E_x = \int_{-\infty}^{\infty} |\tilde{x}(t)|^2 dt \tag{5.3}$$

The following list includes the properties for the radar ambiguity function:

1) The maximum value for the ambiguity function occurs at $(\tau, f_d) = (0, 0)$ and is equal to $4E_x^2$,

$$max\{|\chi(\tau;f_d)|^2\} = |\chi(0;0)|^2 = (2E_x)^2 \tag{5.4}$$

$$|\chi(\tau;f_d)|^2 \le |\chi(0;0)|^2 \tag{5.5}$$

2) The ambiguity function is symmetric,

$$|\chi(\tau;f_d)|^2 = |\chi(-\tau;-f_d)|^2 \tag{5.6}$$

3) The total volume under the ambiguity function is constant,

$$\int\int |\chi(\tau;f_d)|^2 \, d\tau \, df_d = (2E_x)^2 \tag{5.7}$$

4) If the function $X(f)$ is the Fourier transform of the signal $x(t)$, then by using Parseval's theorem we get

$$|\chi(\tau;f_d)|^2 = \left| \int X^*(f) X(f-f_d) e^{-j2\pi f\tau} df \right|^2 \tag{5.8}$$

5) Suppose that $|\chi(\tau;f_d)|^2$ is the ambiguity function for the signal $\tilde{x}(t)$. Adding a quadratic phase modulation term to $\tilde{x}(t)$ yields

$$\tilde{x}_1(t) = \tilde{x}(t) e^{j\pi\mu t^2} \tag{5.9}$$

where μ is a constant. It follows that the ambiguity function for the signal $\tilde{x}_1(t)$ is given by

$$|\chi_1(\tau;f_d)|^2 = |\chi(\tau;(f_d + \mu\tau))|^2 \tag{5.10}$$

5.2. Examples of the Ambiguity Function

The ideal radar ambiguity function is represented by a spike of infinitesimally small width that peaks at the origin and is zero everywhere else, as illustrated in Fig. 5.1. An ideal ambiguity function provides perfect resolution between neighboring targets regardless of how close they may be to each other. Unfortunately, an ideal ambiguity function cannot physically exist because the

ambiguity function must have finite peak value equal to $(2E_x)^2$ and a finite volume also equal to $(2E_x)^2$. Clearly, the ideal ambiguity function cannot meet those two requirements.

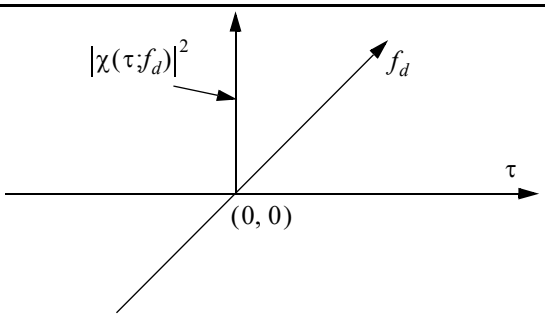

Figure 5.1. Ideal ambiguity function.

5.2.1. Single Pulse Ambiguity Function

The complex envelope of a single pulse is $\tilde{x}(t)$ defined by

$$\tilde{x}(t) = \frac{1}{\sqrt{\tau_0}} Rect\left(\frac{t}{\tau_0}\right) \tag{5.11}$$

From Eq. (5.1) we have

$$\chi(\tau;f_d) = \int_{-\infty}^{\infty} \tilde{x}(t)\tilde{x}^*(t-\tau)e^{j2\pi f_d t}dt \tag{5.12}$$

Substituting Eq. (5.11) into Eq. (5.12) and performing the integration yield

$$|\chi(\tau;f_d)|^2 = \left|\left(1-\frac{|\tau|}{\tau_0}\right)\frac{\sin(\pi f_d(\tau_0-|\tau|))}{\pi f_d(\tau_0-|\tau|)}\right|^2 \qquad |\tau| \le \tau_0 \tag{5.13}$$

Figures 5.2 a and b show 3-D and contour plots of single pulse ambiguity functions. This figure can be reproduced using the following MATLAB code

```
close all; clear all;
eps = 0.000001;
taup = 3;
[x] = single_pulse_ambg (taup);
taux = linspace(-taup,taup, size(x,1));
fdy = linspace(-5/taup+eps,5/taup-eps, size(x,1));
mesh(taux,fdy,x);
```

```
xlabel ('Delay in seconds');
ylabel ('Doppler in Hz');
zlabel ('Ambiguity function')
figure(2)
contour(taux,fdy,x);
xlabel ('Delay in seconds');
ylabel ('Doppler in Hz'); grid
```

The ambiguity function cut along the time-delay axis τ is obtained by setting $f_d = 0$. More precisely,

$$|\chi(\tau;0)| = \left(1 - \frac{|\tau|}{\tau_0}\right)^2 \qquad |\tau| \le \tau_0 \tag{5.14}$$

Note that the time autocorrelation function of the signal $\tilde{x}(t)$ is equal to $\chi(\tau;0)$. Similarly, the cut along the Doppler axis is

$$|\chi(0;f_d)|^2 = \left|\frac{\sin \pi \tau_0 f_d}{\pi \tau_0 f_d}\right|^2 \tag{5.15}$$

Figures 5.3 and 5.4, respectively, show the plots of the uncertainty function cuts defined by Eq. (5.14) and Eq. (5.15). Since the zero Doppler cut along the time-delay axis extends between $-\tau_0$ and τ_0, close targets will be unambiguous if they are at least τ_0 seconds apart.

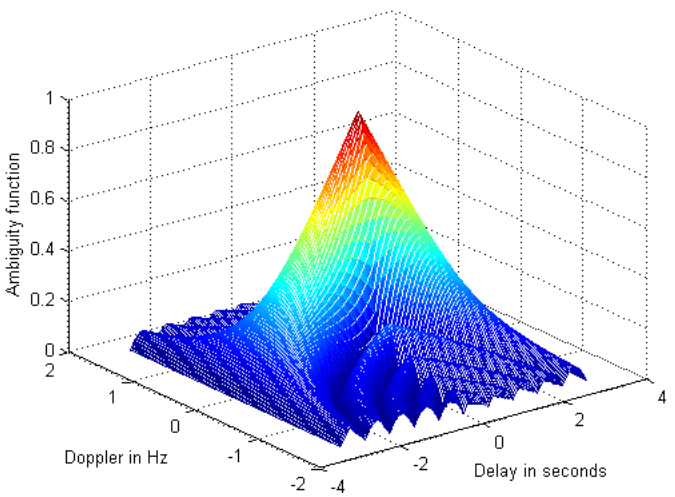

Figure 5.2a. Single pulse 3-D ambiguity plot. Pulse width is 3 seconds.

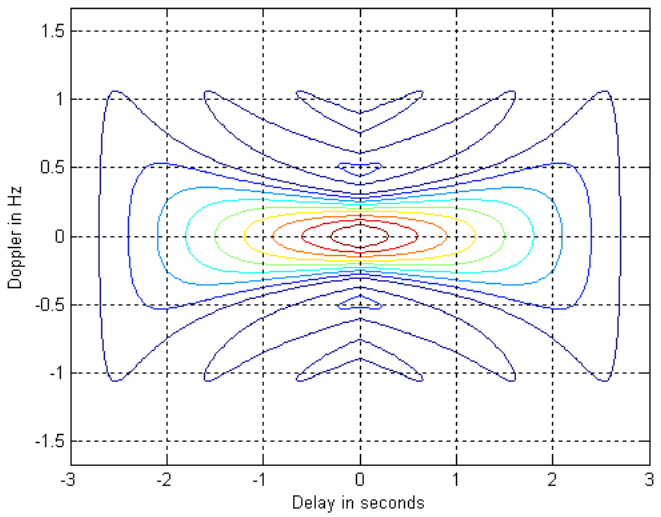

Figure 5.2b. Contour plot corresponding to Fig. 5.2a.

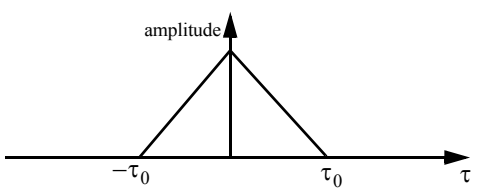

Figure 5.3. Zero Doppler ambiguity function cut along the time-delay axis.

The zero time cut along the Doppler frequency axis has a $(\sin x/x)^2$ shape. It extends from $-\infty$ to ∞. The first null occurs at $f_d = \pm 1/\tau_0$. Hence, it is possible to detect two targets that are shifted by $1/\tau_0$, without any ambiguity. Thus, a single pulse range and Doppler resolutions are limited by the pulse width τ_0. Fine range resolution requires that a very short pulse be used. Unfortunately, using very short pulses requires very large operating bandwidths and may limit the radar average transmitted power to impractical values.

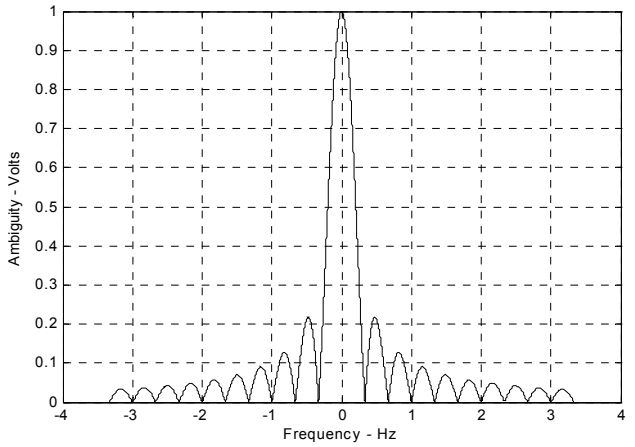

Figure 5.4. Ambiguity function of a single frequency pulse (zero delay). The pulse width is 3 seconds.

5.2.2. LFM Ambiguity Function

Consider the LFM complex envelope signal defined by

$$\tilde{x}(t) = \frac{1}{\sqrt{\tau_0}} Rect\left(\frac{t}{\tau_0}\right) e^{j\pi\mu t^2} \tag{5.16}$$

In order to compute the ambiguity function for the LFM complex envelope, we will first consider the case when $0 \le \tau \le \tau_0$. In this case the integration limits are from $-\tau_0/2$ to $(\tau_0/2) - \tau$. Substituting Eq. (5.16) into Eq. (5.1) yields

$$\chi(\tau; f_d) = \frac{1}{\tau_0} \int_{-\infty}^{\infty} Rect\left(\frac{t}{\tau_0}\right) Rect\left(\frac{t-\tau}{\tau_0}\right) e^{j\pi\mu t^2} e^{-j\pi\mu(t-\tau)^2} e^{j2\pi f_d t} dt \tag{5.17}$$

It follows that

$$\chi(\tau; f_d) = \frac{e^{-j\pi\mu\tau^2}}{\tau_0} \int_{\frac{-\tau_0}{2}}^{\frac{\tau_0}{2}-\tau} e^{j2\pi(\mu\tau + f_d)t} dt \tag{5.18}$$

Finishing the integration process in Eq. (5.18) yields

$$\chi(\tau;f_d) = e^{j\pi\tau f_d}\left(1-\frac{\tau}{\tau_0}\right)\frac{\sin\left(\pi\tau_0(\mu\tau+f_d)\left(1-\frac{\tau}{\tau_0}\right)\right)}{\pi\tau_0(\mu\tau+f_d)\left(1-\frac{\tau}{\tau_0}\right)} \qquad 0\le\tau\le\tau_0 \qquad \textbf{(5.19)}$$

Similar analysis for the case when $-\tau_0 \le \tau \le 0$ can be carried out, where, in this case, the integration limits are from $(-\tau_0/2)-\tau$ to $\tau_0/2$. The same result can be obtained by using the symmetry property of the ambiguity function ($|\chi(-\tau,-f_d)| = |\chi(\tau,f_d)|$). It follows that an expression for $\chi(\tau;f_d)$ that is valid for any τ is given by

$$\chi(\tau;f_d) = e^{j\pi\tau f_d}\left(1-\frac{|\tau|}{\tau_0}\right)\frac{\sin\left(\pi\tau_0(\mu\tau+f_d)\left(1-\frac{|\tau|}{\tau_0}\right)\right)}{\pi\tau_0(\mu\tau+f_d)\left(1-\frac{|\tau|}{\tau_0}\right)} \qquad |\tau|\le\tau_0 \qquad \textbf{(5.20)}$$

and the LFM ambiguity function is

$$|\chi(\tau;f_d)|^2 = \left|\left(1-\frac{|\tau|}{\tau_0}\right)\frac{\sin\left(\pi\tau_0(\mu\tau+f_d)\left(1-\frac{|\tau|}{\tau_0}\right)\right)}{\pi\tau_0(\mu\tau+f_d)\left(1-\frac{|\tau|}{\tau_0}\right)}\right|^2 \qquad |\tau|\le\tau_0 \qquad \textbf{(5.21)}$$

Again the time autocorrelation function is equal to $\chi(\tau,0)$. The reader can verify that the ambiguity function for a down-chirp LFM waveform is given by

$$|\chi(\tau;f_d)|^2 = \left|\left(1-\frac{|\tau|}{\tau_0}\right)\frac{\sin\left(\pi\tau_0(\mu\tau-f_d)\left(1-\frac{|\tau|}{\tau_0}\right)\right)}{\pi\tau_0(\mu\tau-f_d)\left(1-\frac{|\tau|}{\tau_0}\right)}\right|^2 \qquad |\tau|\le\tau_0 \qquad \textbf{(5.22)}$$

Incidentally, either Eq. (5.21) or (5.22) can be obtained from Eq. (5.13) by applying property 5 from Section 5.1. Figures 5.5 a and b show 3-D and contour plots for the LFM uncertainty and ambiguity functions for $\tau_0 = 1$ second and $B = 5Hz$ for a down-chirp pulse. This figure can be reproduced using the following MATLAB code.

```
% Use this program to reproduce Fig. 5.5 of text
close all;
clear all;
eps = 0.0001;
taup = 1.;
b = 5.;
up_down = -1.;
x = lfm_ambg(taup, b, up_down);
```

```
taux = linspace(-1.*taup,taup,size(x,1));
fdy = linspace(-1.5*b,1.5*b,size(x,1));
figure(1)
mesh(taux,fdy,sqrt(x))
xlabel ('Delay in seconds')
ylabel ('Doppler in Hz')
zlabel ('Ambiguity function')
axis tight
figure(2)
contour(taux,fdy,sqrt(x))
xlabel ('Delay in seconds')
ylabel ('Doppler in Hz')
grid
```

The up-chirp ambiguity function cut along the time delay axis τ is

$$|\chi(\tau;0)|^2 = \left| \left(1 - \frac{|\tau|}{\tau_0}\right) \frac{\sin\left(\pi\mu\tau\tau_0\left(1 - \frac{|\tau|}{\tau_0}\right)\right)}{\pi\mu\tau\tau_0\left(1 - \frac{|\tau|}{\tau_0}\right)} \right|^2 \qquad |\tau| \le \tau_0 \tag{5.23}$$

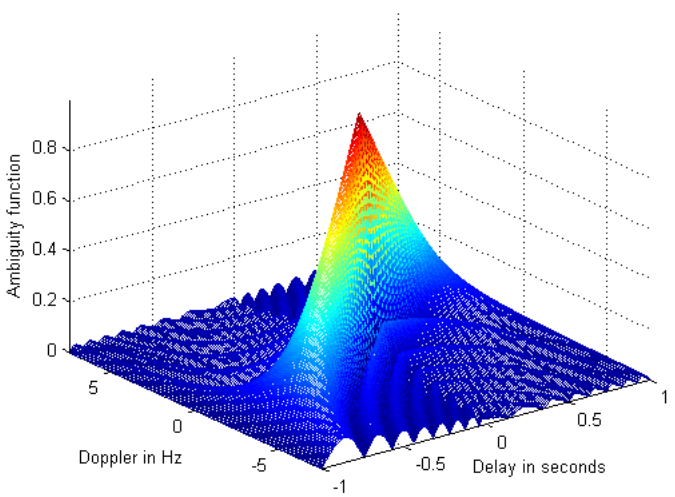

Figure 5.5a. Down-chirp LFM 3-D ambiguity plot. Pulse width is 1 second; and bandwidth is 5 Hz.

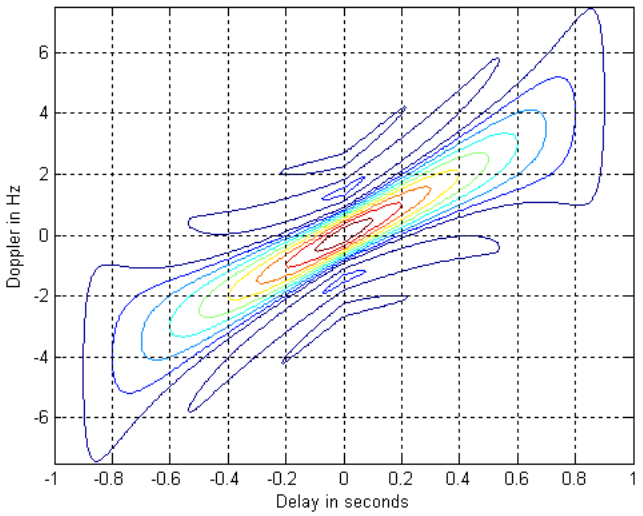

Figure 5.5b. Contour plot corresponding to Fig. 5.5a.

Note that the LFM ambiguity function cut along the Doppler frequency axis is similar to that of the single pulse. This should not be surprising since the pulse shape has not changed (only frequency modulation was added). However, the cut along the time-delay axis changes significantly. It is now much narrower compared to the unmodulated pulse cut. In this case, the first null occurs at

$$\tau_{n1} \approx 1/B \tag{5.24}$$

Figure 5.6 shows a plot for a cut in the uncertainty function corresponding to Eq. (5.23). This figure can be reproduced using the following MATLAB code

```
close all; clear all;
taup = 1;
b =20.;
up_down = 1.;
taux = -1.5*taup:.01:1.5*taup;
mu = up_down * b / 2. / taup;
ii = 0.;
for tau = -1.5*taup:.01:1.5*taup
  ii = ii + 1;
  val1 = 1. - abs(tau) / taup;
  val2 = pi * taup * (1.0 - abs(tau) / taup);
```

```
   val3 = (0 + mu * tau);
   val = val2 * val3;
   x(ii) = abs( val1 * (sin(val+eps)/(val+eps)));
end
figure(1)
plot(taux,10*log10(x+0.001))
grid
xlabel ('Delay in seconds')
ylabel ('Ambiguity in dB')
axis tight
```

Equation (5.24) indicates that the effective pulse width (compressed pulse width) of the matched filter output is completely determined by the radar bandwidth. It follows that the LFM ambiguity function cut along the time-delay axis is narrower than that of the unmodulated pulse by a factor

$$\xi = \frac{\tau_0}{(1/B)} = \tau_0 B \tag{5.25}$$

ξ is referred to as the compression ratio (also called time-bandwidth product and compression gain). All three names can be used interchangeably to mean the same thing. As indicated by Eq. (5.25) the compression ratio also increases as the radar bandwidth is increased.

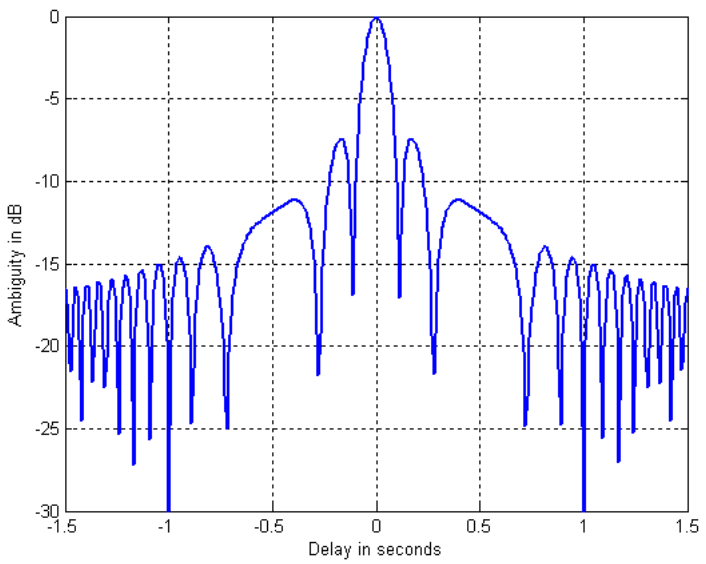

Figure 5.6. Zero Doppler ambiguity of an LFM pulse ($\tau_0 = 1$, $b = 20$).

Example:

Compute the range resolution before and after pulse compression corresponding to an LFM waveform with the following specifications: Bandwidth $B = 1GHz$ *and pulse width* $\tau_0 = 10ms$.

Solution:

The range resolution before pulse compression is

$$\Delta R_{uncomp} = \frac{c\tau_0}{2} = \frac{3 \times 10^8 \times 10 \times 10^{-3}}{2} = 1.5 \times 10^6 \ \ meters$$

Using Eq. (5.23) yields

$$\tau_{n1} = \frac{1}{1 \times 10^9} = 1 \ \ ns$$

$$\Delta R_{comp} = \frac{c\tau_{n1}}{2} = \frac{3 \times 10^8 \times 1 \times 10^{-9}}{2} = 15 \ \ cm$$

5.2.3. Coherent Pulse Train Ambiguity Function

Figure 5.7 shows a plot of a coherent pulse train. The pulse width is denoted as τ_0 and the PRI is T. The number of pulses in the train is N; hence, the train's length is $(N-1)T$ seconds. A normalized individual pulse $\tilde{x}(t)$ is defined by

$$\tilde{x}_1(t) = \frac{1}{\sqrt{\tau_0}} Rect\left(\frac{t}{\tau_0}\right) \tag{5.26}$$

When coherency is maintained between the consecutive pulses, then an expression for the normalized train is

$$\tilde{x}(t) = \frac{1}{\sqrt{N}} \sum_{i=0}^{N-1} \tilde{x}_1(t - iT) \tag{5.27}$$

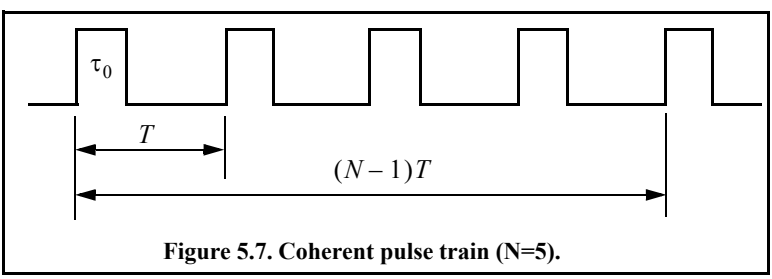

Figure 5.7. Coherent pulse train (N=5).

The output of the matched filter is

$$\chi(\tau;f_d) = \int_{-\infty}^{\infty} \tilde{x}(t)\tilde{x}^*(t-\tau)e^{j2\pi f_d t}dt \tag{5.28}$$

Substituting Eq. (5.27) into Eq. (5.28) and interchanging the summations and integration yield

$$\chi(\tau;f_d) = \frac{1}{N}\sum_{i=0}^{N-1}\sum_{j=0}^{N-1}\int_{-\infty}^{\infty}\tilde{x}_1(t-iT)\ \tilde{x}_1{}^*(t-jT-\tau)e^{j2\pi f_d t}dt \tag{5.29}$$

Making the change of variable $t_1 = t - iT$ yields

$$\chi(\tau;f_d) = \frac{1}{N}\sum_{i=0}^{N-1} e^{j2\pi f_d iT}\sum_{j=0}^{N-1}\int_{-\infty}^{\infty}\tilde{x}_1(t_1)\ \tilde{x}_1{}^*(t_1-[\tau-(i-j)T])e^{j2\pi f_d t_1}dt_1 \tag{5.30}$$

The integral inside Eq. (5.30) represents the output of the matched filter for a single pulse, and is denoted by χ_1. It follows that

$$\chi(\tau;f_d) = \frac{1}{N}\sum_{i=0}^{N-1} e^{j2\pi f_d iT}\sum_{j=0}^{N-1}\chi_1[\tau-(i-j)T;f_d] \tag{5.31}$$

When the relation $q = i-j$ is used, then the following relation is true:

$$\sum_{i=0}^{N}\sum_{m=0}^{N} = \sum_{q=-(N-1)}^{0}\sum_{i=0}^{N-1-|q|}\Bigg|_{for\ j=i-q} + \sum_{q=1}^{N-1}\sum_{j=0}^{N-1-|q|}\Bigg|_{for\ i=j+q} \tag{5.32}$$

Substituting Eq. (5.32) into Eq. (5.31) gives

$$\chi(\tau;f_d) = \frac{1}{N}\sum_{q=-(N-1)}^{0}\left\{\chi_1(\tau-qT;f_d)\sum_{i=0}^{N-1-|q|}e^{j2\pi f_d iT}\right\} \tag{5.33}$$

$$+\frac{1}{N}\sum_{q=1}^{N-1}\left\{e^{j2\pi f_d qT}\chi_1(\tau-qT;f_d)\sum_{j=0}^{N-1-|q|}e^{j2\pi f_d jT}\right\}$$

Setting $z = \exp(j2\pi f_d T)$, and using the relation

$$\sum_{j=0}^{N-1-|q|} z^j = \frac{1-z^{N-|q|}}{1-z} \tag{5.34}$$

yield

$$\sum_{i=0}^{N-1-|q|} e^{j2\pi f_d iT} = e^{[j\pi f_d(N-1-|q|T)]} \frac{\sin[\pi f_d(N-1-|q|)T]}{\sin(\pi f_d T)} \tag{5.35}$$

Using Eq. (5.35) in Eq. (5.31) yields two complementary sums for positive and negative q. Both sums can be combined as

$$\chi(\tau;f_d) = \frac{1}{N} \sum_{q=-(N-1)}^{N-1} \chi_1(\tau - qT;f_d) e^{[j\pi f_d(N-1+q)T]} \frac{\sin[\pi f_d(N-|q|)T]}{\sin(\pi f_d T)} \tag{5.36}$$

The second part of the right-hand side of Eq. (5.36) is the impact of the train on the ambiguity function; while the first part is primarily responsible for its shape details (according to the pulse type being used).

Finally, the ambiguity function associated with the coherent pulse train is computed as the modulus square of Eq. (5.36). For $\tau_0 < T/2$, the ambiguity function reduces to

$$|\chi(\tau;f_d)| = \frac{1}{N} \sum_{q=-(N-1)}^{N-1} |\chi_1(\tau - qT;f_d)| \left|\frac{\sin[\pi f_d(N-|q|)T]}{\sin(\pi f_d T)}\right| \;;|\tau| \le NT \tag{5.37}$$

Within the region $|\tau| \le \tau_0 \Rightarrow q = 0$, Eq. (5.37) can be written as

$$|\chi(\tau;f_d)| = |\chi_1(\tau;f_d)| \left|\frac{\sin[\pi f_d NT]}{N\sin(\pi f_d T)}\right| \;;|\tau| \le \tau_0 \tag{5.38}$$

Thus, the ambiguity function for a coherent pulse train is the superposition of the individual pulse's ambiguity functions. The ambiguity function cuts along the time delay and Doppler axes are, respectively, given by

$$|\chi(\tau;0)|^2 = \left| \sum_{q=-(N-1)}^{N-1} \left(1 - \frac{|q|}{N}\right)\left(1 - \frac{|\tau - q|T}{\tau_0}\right) \right|^2 ; \; |\tau - qT| < \tau_0 \tag{5.39}$$

$$|\chi(0;f_d)|^2 = \left| \frac{1}{N} \frac{\sin(\pi f_d \tau_0)}{\pi f_d \tau_0} \frac{\sin(\pi f_d NT)}{\sin(\pi f_d T)} \right|^2 \tag{5.40}$$

Figures 5.8a and 5.8b show the 3-D ambiguity plot and the corresponding contour plot for $N = 5$, $\tau_0 = 0.4$, and $T = 1$. This plot can be reproduced using the following MATLAB code.

```
clear all; close all;
taup = 0.4; pri = 1; n = 5;
x = train_ambg(taup, n, pri);
figure(1)
time = linspace(-(n-1)*pri-taup, n*pri-taup, size(x,2));
doppler = linspace(-1/taup, 1/taup, size(x,1));
surf(time, doppler, x); %mesh(time, doppler, x);
xlabel('Delay in seconds');  ylabel('Doppler in Hz');
zlabel('Ambiguity function'); axis tight;
figure(2)
contour(time, doppler, (x)); % surf(time, doppler, x);
xlabel('Delay in seconds');  ylabel('Doppler in Hz'); grid; axis tight;
```

Figures 5.8c and 5.8d, respectively shows sketches of the zero Doppler and zero delay cuts in the ambiguity function. The ambiguity function peaks along the frequency axis are located at multiple integers of the frequency $f = 1/T$. Alternatively, the peaks are at multiple integers of T along the delay axis. Width of the ambiguity function peaks along the delay axis is $2\tau_0$. The peak width along the Doppler axis is $1/(N-1)T$.

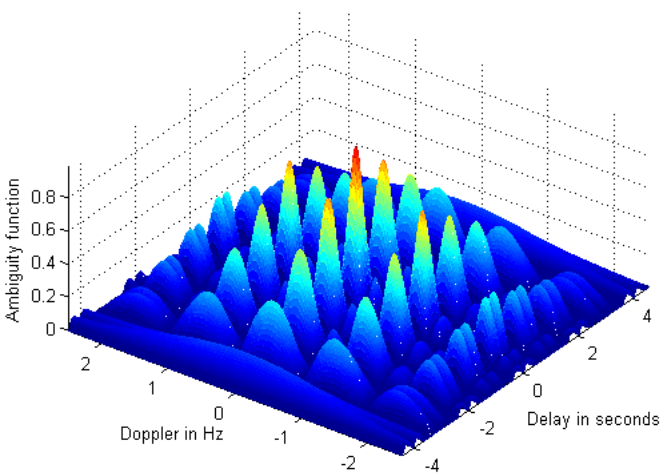

Figure 5.8a. Three-dimensional ambiguity plot for a five-pulse equal amplitude coherent train. Pulse width is 0.4 seconds; and PRI is 1 second, N=5.

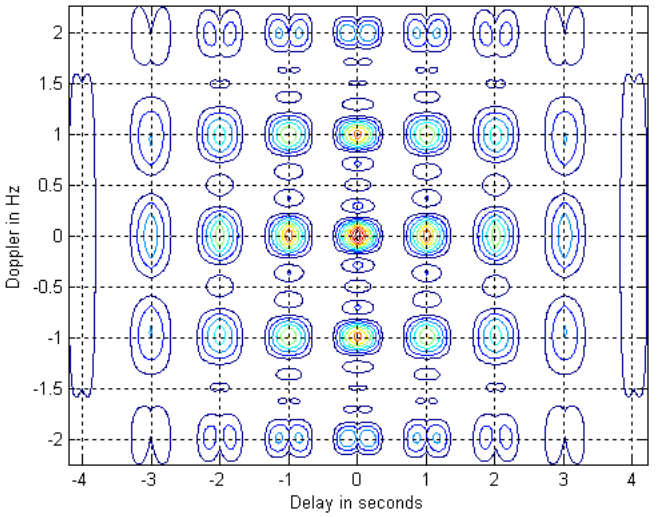

Figure 5.8b. Contour plot corresponding to Fig. 5.8a.

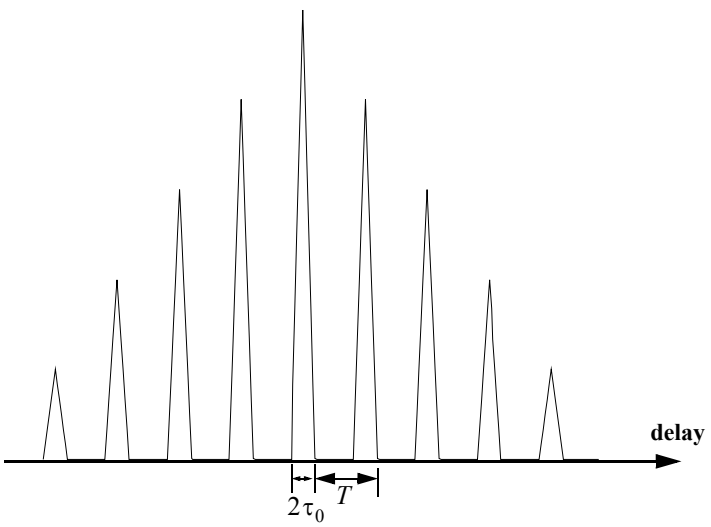

Figure 5.8c. Zero Doppler cut corresponding to Fig. 5.8a.

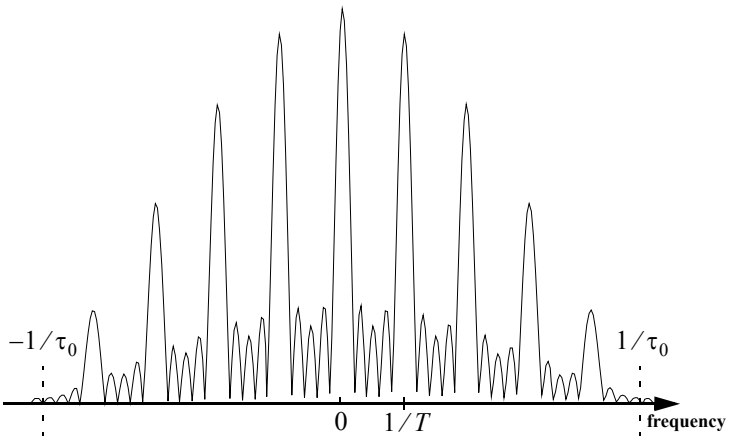

Figure 5.8d. Zero delay cut corresponding to Fig. 5.8a.

5.2.4. Pulse Train Ambiguity Function with LFM

In this case, the signal is as given in the previous section except for the LFM modulation within each pulse. This is illustrated in Fig. 5.9. Again let the pulse width be denoted by τ_0 and the PRI by T. The number of pulses in the train is N; hence, the train's length is $(N-1)T$ seconds. A normalized individual pulse $\tilde{x}_1(t)$ is defined by

$$\tilde{x}_1(t) = \frac{1}{\sqrt{\tau_0}} Rect\left(\frac{t}{\tau_0}\right) e^{j\pi\frac{B}{\tau_0}t^2} \tag{5.41}$$

where B is the LFM bandwidth.

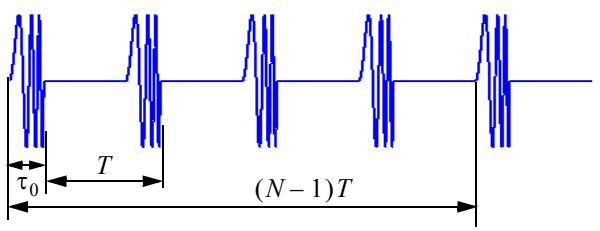

Figure 5.9. LFM pulse train (N=5).

The signal is now given by

$$\tilde{x}(t) = \frac{1}{\sqrt{N}} \sum_{i=0}^{N-1} \tilde{x}_1(t - iT) \tag{5.42}$$

Utilizing property 5 of Section 5.1 and Eq. (5.37) yields the following ambiguity function

$$\left|\chi(\tau; f_d)\right| = \sum_{q=-(N-1)}^{N-1} \left|\chi_1\left(\tau - qT; f_d + \frac{B}{\tau_0}\tau\right)\right| \left|\frac{\sin[\pi f_d (N - |q|)T]}{N \sin(\pi f_d T)}\right| \quad ; |\tau| \le NT \tag{5.43}$$

where χ_1 is the ambiguity function of the single pulse. Note that the shape of the ambiguity function is unchanged from the case of unmodulated train along the delay axis. This should be expected since only a phase modulation has been added which will impact the shape only along the frequency axis.

Figures 5.10 a and b show the ambiguity plot and its associated contour plot for the same example listed in the previous section except, in this case, LFM modulation is added and $N = 3$ pulses. This figure can be reproduced using the following MATLAB code.

```
% figure 5.10
clear all; close all;
taup = 0.4;
pri = 1;
n = 3;
bw = 10;
x = train_ambg_lfm(taup, n, pri, bw);
figure(1)
time = linspace(-(n-1)*pri-taup, n*pri-taup, size(x,2));
doppler = linspace(-bw,bw, size(x,1));
%mesh(time, doppler, x);
surf(time, doppler, x); shading interp;
xlabel('Delay in seconds');
ylabel('Doppler in Hz');
zlabel('Ambiguity function');
axis tight;
title('LFM pulse train, B\tau = 40, N = 3 pulses')
figure(2)
contour(time, doppler, (x));
%surf(time, doppler, x); shading interp; view(0,90);
xlabel('Delay in seconds');
ylabel('Doppler in Hz');
grid; axis tight;
title('LFM pulse train, B\tau = 40, N = 3 pulses')
```

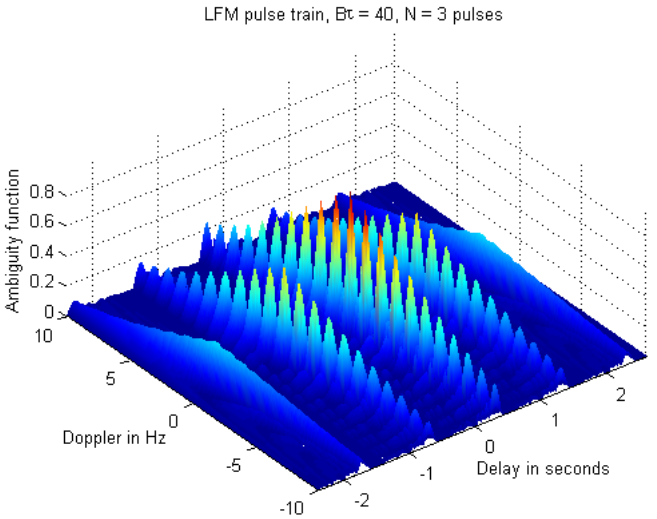

Figure 5.10a. Three-dimensional ambiguity plot for an LFM pulse train.

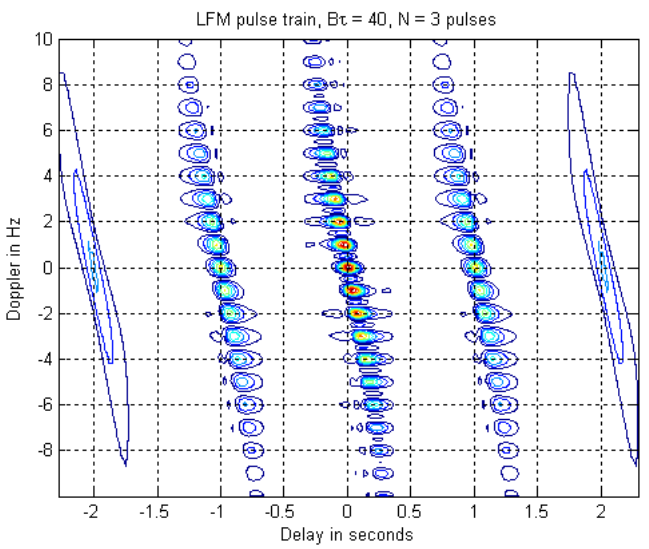

Figure 5.10b. Contour plot corresponding to Fig. 5.10a.

Understanding the difference between the ambiguity diagrams for a coherent pulse train and an LFM pulse train can be done with the help of Fig. 5.11a and Fig. 5.11b. In both figures a train of three pulses is used; in both cases the pulse width is $\tau_0 = 0.4\,sec$ and the period is $T = 1\,sec$. In the case, of LFM pulse train each pulse has LFM modulation with $B\tau_0 = 20$. Locations of the ambiguity peaks along the delay and Doppler axes are the same in both cases. This is true because peaks along the delay axis are T seconds apart and peaks along the Doppler axis are $1/T$ apart; in both cases T is unchanged. Additionally, the width of the ambiguity peaks along the Doppler axis are also the same in both cases, because this value depends only on the pulse train length which is the same in both cases (i.e., $(N-1)T$).

Width of the ambiguity peaks along the delay axis are significantly different, however. In the case of coherent pulse train, this width is approximately equal to twice the pulse width. Alternatively, this value is much smaller in the case of the LFM pulse train. The ratio between the two values is as given in Eq. (5.25). This clearly leads to the expected conclusion that the addition of LFM modulation significantly enhances the range resolution. Finally, the presence of the LFM modulation introduces a slope change in the ambiguity diagram; again a result that is also expected.

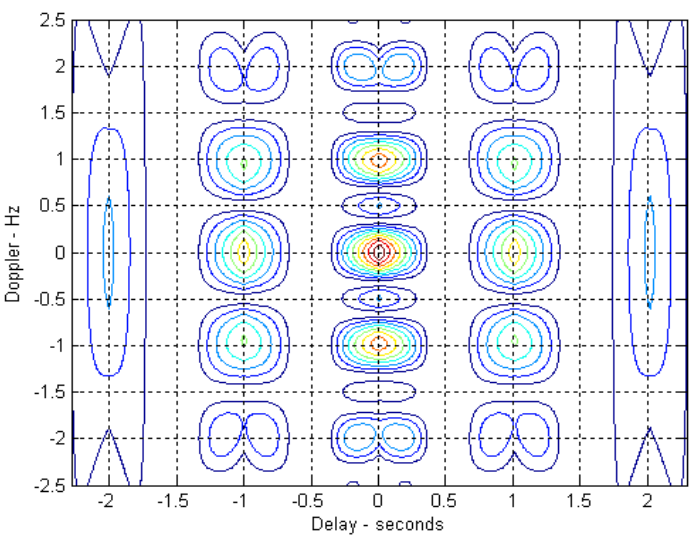

Figure 5.11a. Contour plot for the ambiguity function of a coherent pulse train. $N = 3; \tau_0 = 0.4;\ T = 1$

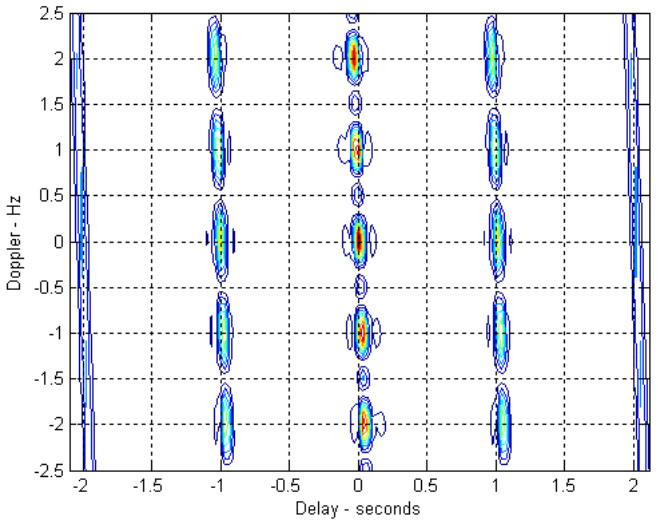

Figure 5.11b. Contour plot for the ambiguity function of a coherent pulse train. $N = 3;\ B\tau_0 = 20;\ T = 1$

5.3. Stepped Frequency Waveforms

Stepped Frequency Waveforms (SFW) is a class of radar waveforms that are used in extremely wide bandwidth applications where very large time bandwidth product (or compression ratio as defined in Eq. (5.25)) is required. One may think of SFW as a special case of an extremely wide bandwidth LFM waveform. For this purpose, consider an LFM signal whose bandwidth is B_i and whose pulsewidth is T_i and refer to it as the primary LFM. Divide this long pulse into N subpulses each of width τ_0 to generate a sequence of pulses whose PRI is denoted by T. It follows that $T_i = (n-1)T$. One reason SFW is favored over an extremely wideband LFM is that it may be very difficult to maintain the LFM slope when the time bandwidth product is large. By using SFW, the same equivalent bandwidth can be achieved; however, phase errors are minimized since the LFM is chirped over a much shorter duration.

Define the beginning frequency for each subpulse as that value measured from the primary LFM at the leading edge of each subpulse, as illustrated in Fig. 5.12. That is

$$f_i = f_0 + i\Delta f;\ \ i = 0, N-1 \qquad \textbf{(5.44)}$$

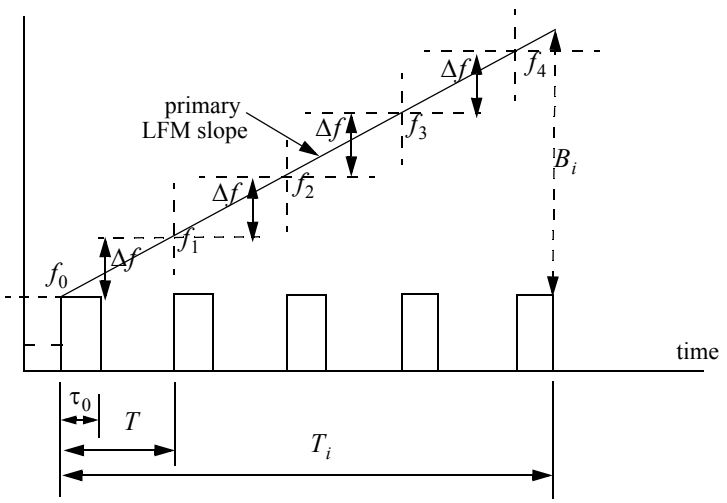

Figure 5.12. Example of stepped frequency waveform burst; $N = 5$.

where Δf is the frequency step from one subpulse to another. The set of n subpulses is often referred to as a burst. Each subpulse can have its own LFM modulation. To this end, assume that the subpulse LFM modulation corresponds to an LFM slope of $\mu = B/\tau_0$.

The complex envelope of a single subpluse with LFM modulation is

$$\tilde{x}_1 = \frac{1}{\sqrt{\tau_0}} Rect\left(\frac{t}{\tau_0}\right) e^{j\pi\mu t^2} \tag{5.45}$$

Of course if the subpulses do not have any LFM modulation, then the same equation holds true by setting $\mu = 0$. The overall complex envelope of the whole burst is

$$\tilde{x}(t) = \frac{1}{\sqrt{N}} \sum_{i=0}^{N-1} \tilde{x}_1(t - iT) \tag{5.46}$$

The ambiguity function of the matched filter corresponding to Eq. (5.46) can be obtained from that of the coherent pulse train developed in Section 5.2.3 along with property 5 of the ambiguity function. The details are fairly straightforward and are left to the reader as an exercise. The result is (see Problem 5.2)

$$|\chi(\tau;f_d)| = \sum_{q=-(N-1)}^{N-1} \left|\chi_1\left(\tau - qT;\left(f_d + \frac{B}{\tau_0}\tau\right)\right)\right| \times \left|\frac{\sin\left[\pi\left(f_d + \frac{\Delta f}{T}\tau\right)(N-|q|)T\right]}{N\sin\left(\pi\left(f_d + \frac{\Delta f}{T}\tau\right)T\right)}\right| ;|\tau| \le NT \quad (5.47)$$

where χ_1 is the ambiguity function of the single pulse. Unlike the case in Eq. (5.43), the second part of the right-hand side of Eq. (5.47) is now modified according to property 5 of Section 5.1. This is true since each subpulse has its own beginning frequency derived from the primary LFM slope.

5.4. Nonlinear FM

As clearly shown by Fig. 5.6 the output of the matched filter corresponding to an LFM pulse has sidelobe levels similar to those of the $\sin(x)/x$ signal, that is, 13.4 dB below the main beam peak. In many radar applications, these sidelobe levels are considered too high and may present serious problems for detection particularly in the presence of nearby interfering targets or other noise sources. Therefore, in most radar applications, sidelobe reduction of the output of the matched filter is always required. This sidelobe reduction can be accomplished using windowing techniques as described in Chapter 2. However, windowing techniques reduce the sidelobe levels at the expense of reducing of the SNR and widening the main beam (i.e., loss of resolution) which are considered to be undesirable features in many radar applications.

These effects can be mitigated by using non-linear FM (NLFM) instead of LFM waveforms. In this case, the LFM waveform spectrum is shaped according to a specific predetermined frequency function. Effectively, in NLFM, the rate of change of the LFM waveform phase is varied so that less time is spent on the edges of the bandwidth, as illustrated in Fig. 5.13. The concept of NLFM can be better analyzed and understood in the context of the stationary phase.

5.4.1. The Concept of Stationary Phase

Consider the following bandpass signal

$$x(t) = x_I(t)\cos(2\pi f_0 t + \phi(t)) - x_Q(t)\sin(2\pi f_0 t + \phi(t)) \quad (5.48)$$

where $\phi(t)$ is the frequency modulation. The corresponding analytic signal (pre-envelope) is

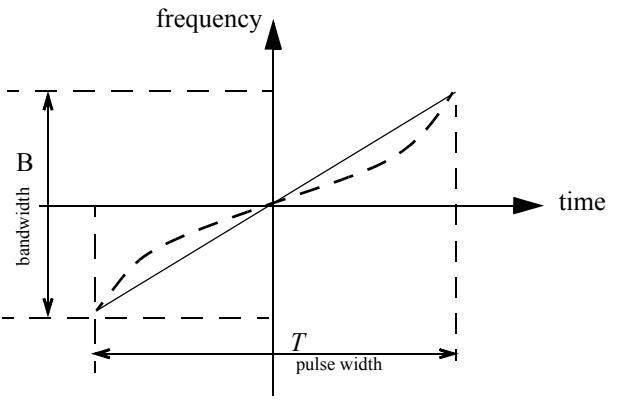

Figure 5.13. A cartoon showing frequency versus time for an LFM waveform (solid line) and a NLFM (dashed line).

$$\psi(t) = \tilde{x}(t)e^{j2\pi f_0 t} = r(t)e^{j\phi(t)}e^{j2\pi f_0 t} \tag{5.49}$$

where $\tilde{x}(t)$ is the complex envelope and is given by

$$\tilde{x}(t) = r(t)e^{j\phi(t)} \tag{5.50}$$

The lowpass signal $r(t)$ represents the envelope of the transmitted signal; it is given by

$$r(t) = \sqrt{x_I^2(t) + x_Q^2(t)} \tag{5.51}$$

It follows that the FT of the signal $\tilde{x}(t)$ can then be written as

$$X(\omega) = \int_{-\infty}^{\infty} r(t)e^{j(-\omega t + \phi(t))}\, dt \tag{5.52}$$

$$X(\omega) = |X(\omega)|e^{j\Phi(\omega)} \tag{5.53}$$

where $|X(\omega)|$ is the modulus of the FT and $\Phi(\omega)$ is the corresponding phase frequency response. It is clear that the integrand is an oscillating function of time varying at a rate

$$\frac{d}{dt}[\omega t - \phi(t)] \tag{5.54}$$

Most contribution to the FT spectrum occurs when this rate of change is minimal. More specifically, it occurs when

$$\frac{d}{dt}[\omega t - \phi(t)] = 0 \Rightarrow \omega - \phi'(t) = 0 \tag{5.55}$$

The expression in Eq. (5.55) is parametric since it relates two independent variables. Thus, for each value ω_n there is only one specific $\phi'(t_n)$ that satisfies Eq. (5.55). Thus, the time when this phase term is stationary will be different for different values of ω_n. Expanding the phase term in Eq. (5.55) about an incremental value t_n using Taylor series expansion yields

$$\omega_n t - \phi(t) = \omega_n t_n - \phi(t_n) + (\omega_n - \phi'(t_n))(t - t_n) - \frac{\phi''(t_n)}{2!}(t - t_n)^2 + \ldots \tag{5.56}$$

An acceptable approximation of Eq. (5.56) is obtained by using the first three terms, provided that the difference $(t - t_n)$ is very small. Now, using the right-hand side of Eq. (5.55) into Eq. (5.56) and terminating the expansion to the first three terms yield

$$\omega_n t - \phi(t) = \omega_n t_n - \phi(t_n) - \frac{\phi''(t_n)}{2!}(t - t_n)^2 \tag{5.57}$$

By substituting Eq. (5.57) into Eq. (5.52) and using the fact that $r(t)$ is relatively constant (slow varying) when compared to the rate at which the carrier signal is varying, gives

$$X(\omega_n) = r(t_n) \int_{t_n^-}^{t_n^+} e^{-j\left(\omega_n t_n - \phi(t_n) - \frac{\phi''(t_n)}{2}(t - t_n)^2\right)} \, dt \tag{5.58}$$

where t_n^+ and t_n^- represent infinitesimal changes about t_n. Equation (5.58) can be written as

$$X(\omega_n) = r(t_n) e^{j(-\omega_n t_n - \phi(t_n))} \int_{t_n^-}^{t_n^+} e^{j\left(\frac{\phi''(t_n)}{2}(t - t_n)^2\right)} \, dt \tag{5.59}$$

Consider the changes of variables

$$t - t_n = \lambda \Rightarrow dt = d\lambda \tag{5.60}$$

$$\sqrt{\phi''(t_n)}\lambda = \sqrt{\pi}\, y \Rightarrow d\lambda = \frac{\sqrt{\pi}}{\sqrt{\phi''(t_n)}} dy \tag{5.61}$$

Using these changes of variables leads to

$$X(\omega_n) = \frac{2\sqrt{\pi}\ r(t_n)}{\sqrt{\phi''(t_n)}} e^{j(-\omega_n t_n - \phi(t_n))} \int_0^{y_0} e^{j\left(\frac{\pi y^2}{2}\right)}\ dy \tag{5.62}$$

where

$$y_0 = \sqrt{\frac{|\phi''(t_n)|}{\pi}} \tag{5.63}$$

The integral in Eq. (5.62) is that of the form of a Fresnel integral, which has an upper limit approximated by

$$\frac{\exp\left(j\frac{\pi}{4}\right)}{\sqrt{2}} \tag{5.64}$$

Substituting Eq. (5.64) into Eq. (5.62) yields

$$X(\omega_n) = \frac{\sqrt{2\pi}\ r(t_n)}{\sqrt{\phi''(t_n)}} e^{j\left(-\omega_n t_n - \phi(t_n) + \frac{\pi}{4}\right)} \tag{5.65}$$

Thus, for all possible values of ω

$$|X(\omega_t)|^2 \approx 2\pi \frac{r^2(t)}{|\phi''(t)|} \Rightarrow |X(\omega)| = \frac{\sqrt{2\pi}}{\sqrt{|\phi''(t)|}}\ r(t) \tag{5.66}$$

The subscript t was used to indicate the dependency of ω on time.

Using a similar approach that led to Eq. (5.66), an expression for $\tilde{x}(t_n)$ can be obtained. From Eq. (5.53), the signal $\tilde{x}(t)$

$$\tilde{x}(t) = \frac{1}{2\pi} \int_{-\infty}^{\infty} |X(\omega)|\ e^{j(\Phi(\omega) + \omega t)}\ d\omega \tag{5.67}$$

The phase term $\Phi(\omega)$ is (using Eq. (5.65))

$$\Phi(\omega) = -\omega t - \phi(t) + \frac{\pi}{4} \tag{5.68}$$

Differentiating with respect to ω yields

$$\frac{d}{d\omega}\Phi(\omega) = -t - \left(\frac{dt}{d\omega}\right)\left[\omega - \frac{d}{dt}\phi(t)\right] = \Phi'(\omega) \tag{5.69}$$

Using the stationary phase relation in Eq. (5.55) (i.e., $\omega - \phi'(t) = 0$) yields

$$\Phi'(\omega) = -t \tag{5.70}$$

and

$$\Phi''(\omega) = -\frac{dt}{d\omega} \tag{5.71}$$

Define the signal group time delay function as

$$T_g(\omega) = -\Phi'(\omega) \tag{5.72}$$

then the signal instantaneous frequency is the inverse of the $T_g(\omega)$. Figure 5.14 shows a drawing illustrating this inverse relationship between the NLFM frequency modulation and the corresponding group time delay function.

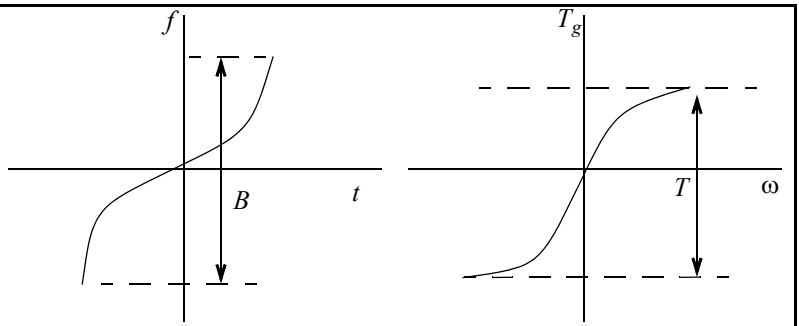

Figure 5.14. Matched filter time delay and frequency modulation for a NLFM waveform.

Comparison of Eq. (5.67) and Eq. (5.52) indicates that both equation have similar form. Thus, if one substitutes $X(\omega)/2\pi$ for $r(t)$, $\Phi(\omega)$ for $\phi(t)$, ω for t, and $-t$ for ω in Eq. (5.52), a similar expression to that in Eq. (5.65) can be derived. That is,

$$\left|\tilde{x}(t_\omega)\right|^2 \approx \frac{1}{2\pi}\frac{\left|X(\omega)\right|^2}{\left|\Phi''(\omega)\right|} \tag{5.73}$$

the subscript ω was used to indicate the dependency of t on frequency. However, from Eq. (5.60)

$$\left|\tilde{x}(t)\right|^2 = \left|r(t)e^{j\phi(t)}\right|^2 = r^2(t) \tag{5.74}$$

It follows that Eq. (5.73) can be rewritten as

$$r^2(t_\omega) \approx \frac{1}{2\pi}\frac{|X(\omega)|^2}{|\Phi''(\omega)|} \Rightarrow r(t) = \frac{|X(\omega)|}{\sqrt{2\pi|\Phi''(\omega)|}} \tag{5.75}$$

substituting Eq. (5.71) into Eq. (5.75) yields a general relationship for any t

$$r^2(t)\ dt = \frac{1}{2\pi}|X(\omega)|^2 d\omega \tag{5.76}$$

Clearly, the functions $r(t)$, $\phi(t)$, $X(\omega)$, and $\Phi(\omega)$ are related to each other as Fourier transform pairs, as given by

$$r(t)e^{j\phi(t)} = \frac{1}{2\pi}\int_{-\infty}^{\infty}|X(\omega)|\ e^{j(\Phi(\omega)+\omega t)}\ d\omega \tag{5.77}$$

$$|X(\omega)|\ e^{j\Phi(\omega)} = \int_{-\infty}^{\infty} r(t)\ e^{-j(\omega t-\phi(t))}\ d\omega \tag{5.78}$$

They are also related using the Parseval's theorem by

$$\int_{-\infty}^{t} r^2(\zeta)\ d\zeta = \frac{1}{2\pi}\int_{\omega}^{\infty}|X(\lambda)|^2\ d\lambda \tag{5.79}$$

or

$$\int_{-\infty}^{t} r^2(\zeta)\ d\zeta = \frac{1}{2\pi}\int_{-\infty}^{\omega}|X(\lambda)|^2\ d\lambda \tag{5.80}$$

The formula for the output of the matched filter was derived earlier and is repeated here as Eq. (5.81)

$$\chi(\tau, f_d) = \int_{-\infty}^{\infty}\tilde{x}(t)\tilde{x}^*(t-\tau)e^{j2\pi f_d t}dt \tag{5.81}$$

Substituting the right-hand side of Eq. (5.50) into Eq. (5.89) yields

$$\chi(\tau, f_d) = \int_{-\infty}^{\infty} r(t)r^*(t-\tau)e^{j2\pi f_d t}dt \tag{5.82}$$

It follows that the zero Doppler and zero delay cuts of the ambiguity function can be written as

$$\chi(\tau, 0) = \frac{1}{2\pi}\int_{-\infty}^{\infty} |X(\omega)|^2 \; e^{j\omega\tau} d\omega \tag{5.83}$$

$$\chi(0, f_d) = \int_{-\infty}^{\infty} |r(t)|^2 \; e^{j2\pi f_d t} dt \tag{5.84}$$

These two equations, imply that the shape of the ambiguity function cuts are controlled by selecting different functions X and r (related as defined in Eq. (5.76)). In other words, the ambiguity function main beam and its delay axis sidelobes can be controlled (shaped) by the specific choices of these two functions; and hence, the term *spectrum shaping* is used. Using this concept of spectrum shaping, one can control the frequency modulation of an LFM (see Fig. 5.13) to produce an ambiguity function with the desired sidelobe levels.

5.4.2. Frequency Modulated Waveform Spectrum Shaping

One class of FM waveforms which takes advantage of the stationary phase principles to control (shape) the spectrum is

$$|X(\omega; n)|^2 = \left(\cos\pi\left(\frac{\pi\omega}{B_n}\right)\right)^n \qquad ; \; |\omega| \le \frac{B_n}{2} \tag{5.85}$$

where the value n is an integer greater than zero. It can be easily shown using direct integration and by utilizing Eq. (5.85) that

$$n = 1 \Rightarrow T_{g1}(\omega) = \frac{T}{2}\sin\left(\frac{\pi\omega}{B_1}\right) \tag{5.86}$$

$$n = 2 \Rightarrow T_{g2}(\omega) = T\left[\frac{\omega}{B_2} + \frac{1}{2\pi}\sin\left(\frac{2\pi\omega}{B_2}\right)\right] \tag{5.87}$$

$$n = 3 \Rightarrow T_{g3}(\omega) = \frac{T}{4}\left\{\sin\left(\frac{\pi\omega}{B_3}\right)\left[\left(\cos\frac{\pi\omega}{B_3}\right)^2 + 2\right]\right\} \tag{5.88}$$

$$n = 4 \Rightarrow T_{g4}(\omega) = T\left\{\frac{\omega}{B_4} + \frac{1}{2\pi}\sin\frac{2\pi\omega}{B_4} + \frac{2}{3\pi}\left(\cos\frac{\pi\omega}{B_4}\right)^3 \sin\frac{\pi\omega}{B_4}\right\} \tag{5.89}$$

Figure 5.15 shows a plot for Eq. (5.86) through Eq. (5.89). These plots assume $T = 1$ and the x-axis is normalized, with respect to B. This figure can be reproduced using the following MATLAB code:

```
% Figure 5.15
clear all; close all;
delw = linspace(-.5,.5,75);
T1 = .5 .* sin(pi.*delw);
T2 = delw + (1/2/pi) .* sin(2*pi.*delw);
T3 = .25 .* (sin(pi.*delw)) .* ((cos(pi.*delw)).^2 + 2);
T4 = delw + (1/2/pi) .* sin(2*pi.*delw) + (2/3/pi) .* (cos(pi.*delw)).^3 .* sin(delw);
figure (1)
plot(delw,T1,'k*',delw,T2,'k:',delw,T3,'k.',delw,T4,'k');
grid
ylabel('Group delay function'); xlabel('\omega/B')
legend('n=1','n=2','n=3','n=4')
```

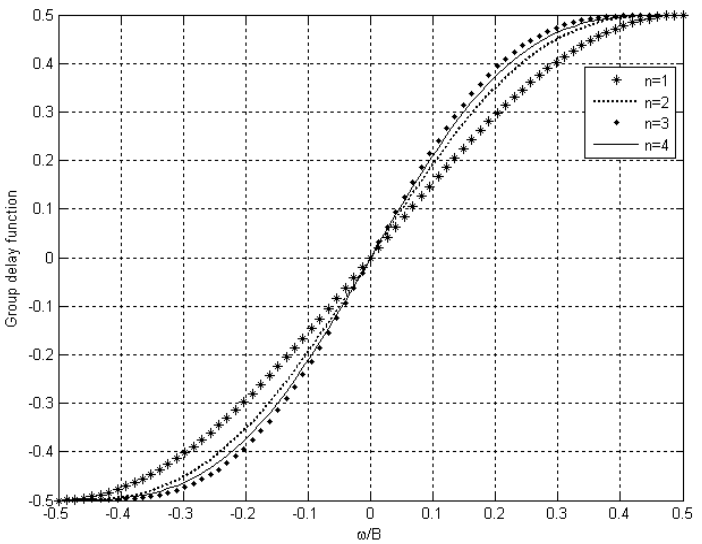

Figure 5.15. Group time delay of Eq. (5.85).

The Doppler mismatch (i.e, a peak of the ambiguity function at a delay value other than zero) is proportional to the amount of Doppler frequency f_d. Hence, an error in measuring target range is always expected when LFM waveforms are used. To achieve sidelobe levels for the output of the matched filter that do not exceed a predetermined level use this class of NLFM waveforms

$$|X(\omega;n;k)|^2 = k + (1-k)\left(\cos\pi\left(\frac{\pi\omega}{B_n}\right)\right)^n \qquad ;|\omega| \le \frac{B_n}{2} \tag{5.90}$$

For example, using the combination $n = 2$, $k = 0.08$ yields sidelobe levels less than $-40dB$.

5.5. Ambiguity Diagram Contours

Plots of the ambiguity function are called ambiguity diagrams. For a given waveform, the corresponding ambiguity diagram is normally used to determine the waveform properties such as the target resolution capability, measurements (time and frequency) accuracy, and its response to clutter. The ambiguity diagram contours are cuts in the 3-D ambiguity plot at some value, Q, such that $Q < |\chi(0, 0)|^2$. The resulting plots are ellipses (see Problem 5.11). The width of a given ellipse along the delay axis is proportional to the signal effective duration, τ_e, defined in Chapter 2. Alternatively, the width of an ellipse along the Doppler axis is proportional to the signal effective bandwidth, B_e.

Figure 5.16 shows a sketch of typical ambiguity contour plots associated with a single unmodulated pulse. As illustrated in Fig. 5.16, narrow pulses provide better range accuracy than long pulses. Alternatively, the Doppler accuracy is better for a wider pulse than it is for a short one. This trade-off between range and Doppler measurements comes from the uncertainty associated with the time-bandwidth product of a single sinusoidal pulse, where the product of uncertainty in time (range) and uncertainty in frequency (Doppler) cannot be much smaller than unity (see Problem 5.12). Figure 5.17 shows the ambiguity contour plot associated with an LFM waveform. The slope is an indication of the LFM modulation. The values σ_τ, σ_{f_d}, $\sigma_{\tau RDC}$, and $\sigma_{f_d RDC}$ were derived in Chapter 4 and were, respectively given in Eq. (4.107), Eq. (4.111), Eq. (4.136), and Eq. (4.137).

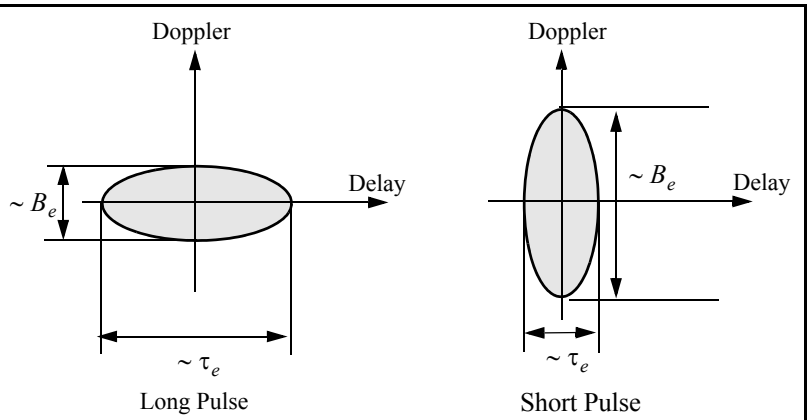

Figure 5.16. Ambiguity contour plot associated with a sinusoid modulated gated CW pulse.

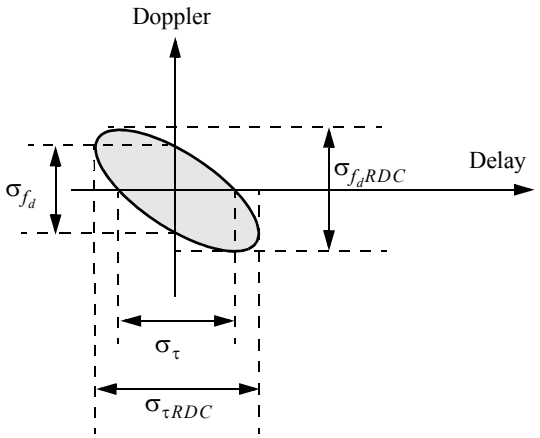

Figure 5.17. Ambiguity contour plot for an up-chirp LFM waveform.

5.6. Interpretation of Range-Doppler Coupling in LFM Signals

An expression of the range-Doppler for LFM signals was derived in Chapter 4. Range-Doppler coupling affects the radar's ability to compute target range and Doppler estimates. An interpretation of this term in the context of the ambiguity function can be explained further with the help of Eq. (5.20). Observation of this equation indicates that ambiguity function for the LFM pulse has a peak value not at $\tau = 0$ but rather at

$$(B/\tau_0)\tau - f_d = 0 \Rightarrow \tau = f_d - \tau_0/B \qquad \textbf{(5.91)}$$

This Doppler mismatch (i.e, a peak of the ambiguity function at a delay value other than zero) is proportional to the amount of Doppler frequency f_d. Hence, an error in measuring target range is always expected when LFM waveforms are used.

Most radar systems using LFM waveforms will correct for the effect of range-Doppler coupling by repeating the measurement with an LFM waveform of the opposite slope and averaging the two measurements. This way, the range measurement error is negated and the true target range is extracted from the averaged value. However, some radar systems, particularly those used for long range surveillance applications, may actually take advantage of range-Doppler coupling effect; and here is how it works: Typically radars during the search mode utilize very wide range bins which may contain many targets with differ-

ent distinct Doppler frequencies. It follows that the output of the matched filter has several targets that have equal delay but different Doppler mismatches.

All targets with Doppler mismatches greater than $1/\tau_0$ are significantly attenuated by the ambiguity function (because of the sharp decaying slope of the ambiguity function along the Doppler axis) and thus will most likely go undetected along the Doppler axis. The combined target complex within that range bin is then detected by the LFM as if all targets had Doppler mismatch corresponding to the target whose Doppler mismatch is less or equal to $1/\tau_0$. Thus, all targets within that wide range bin are detected as one narrowband target. Because of this range-Doppler coupling LFM waveforms are often referred to as Doppler intolerant (insensitive) waveforms.

5.7. MATLAB Programs and Functions

This section presents listings for all the MATLAB programs used to produce all of the MATLAB-generated figures in this chapter. They are listed in the same order in which they appear in the text.

5.7.1. Single Pulse Ambiguity Function

The MATLAB function *"single_pulse_ambg.m"* implements Eq. (5.11). The syntax is as follows:

single_pulse_ambg [taup]

taup is the pulse width.

MATLAB Function** "single_pulse_ambg.m" **Listing

```
function [x] = single_pulse_ambg (taup)
eps = 0.000001;
i = 0;
del = 2*taup/150;
for tau = -taup:del:taup
  i = i + 1;
  j = 0;
  fd = linspace(-5/taup,5/taup,151);
  val1 = 1. - abs(tau) / taup;
  val2 = pi * taup .* (1.0 - abs(tau) / taup) .* fd;
  x(:,i) = abs( val1 .* sin(val2+eps)./(val2+eps));
end
```

5.7.2. LFM Ambiguity Function

The function *"lfm_ambg.m"* implements Eq. (5.20). The syntax is as follows:

lfm_ambg [taup, b, up_down]

where

Symbol	Description	Units	Status
taup	*pulse width*	*seconds*	*input*
b	*bandwidth*	*Hz*	*input*
up_down	*up_down = 1 for up-chirp* *up_down = -1 for down-chirp*	*none*	*input*

MATLAB Function** "lfm_ambg.m" **Listing

```
function [x] = single_pulse_ambg (taup)
% Single umodulated pulse
eps = 0.000001;
i = 0;
del = 2*taup/150;
for tau = -taup:del:taup
   i = i + 1;
  j = 0;
  fd = linspace(-5/taup,5/taup,151);
  val1 = 1. - abs(tau) / taup;
  val2 = pi * taup .* (1.0 - abs(tau) / taup) .* fd;
  x(:,i) = abs( val1 .* sin(val2+eps)./(val2+eps));
end
```

5.7.3. Pulse Train Ambiguity Function

The function *"train_ambg.m"* implements Eq. (5.35). The syntax is as follows:

train_ambg [taup, n, pri]

where

Symbol	Description	Units	Status
taup	*pulse width*	*seconds*	*input*
n	*number of pulses in train*	*none*	*input*
pri	*pulse repetition interval*	*seconds*	*input*

MATLAB Function** "train_ambg.m" **Listing

```
function x = train_ambg(taup, n, pri)
% This code was developed by Stephen Robinson, a senior radar engineer at
% deciBel Research in Hunstville AL
if (taup >= pri/2)
   'ERROR. Pulse width must be less than the PRI/2.'
```

```
   return
end
eps = 1.0e-6;
bw = 1/taup;
q = -(n-1):1:n-1;
offset = 0:0.0533:pri;
[Q, S] = meshgrid(q, offset);
Q = reshape(Q, 1, length(q)*length(offset));
S = reshape(S, 1, length(q)*length(offset));
tau = (-taup * ones(1,length(S))) + S;
fd = -bw:0.033:bw;
[T, F] = meshgrid(tau, fd);
Q = repmat(Q, length(fd), 1);
S = repmat(S, length(fd), 1);
N = n * ones(size(T));
val1 = 1.0-(abs(T))/taup;
val2 = pi*taup*F.*val1;
val3 = abs(val1.*sin(val2+eps)./(val2+eps));
val4 = abs(sin(pi*F.*(N-abs(Q))*pri+eps)./sin(pi*F*pri+eps));
x = val3.*val4./N;
[rows, cols] = size(x);
x = reshape(x, 1, rows*cols);
T = reshape(T, 1, rows*cols);
indx = find(abs(T) > taup);
x(indx) = 0.0;
x = reshape(x, rows, cols);
return
```

5.7.4. Pulse Train Ambiguity Function with LFM

The function *"train_ambg_lfm.m"* implements Eq. (5.43). The syntax is as follows:

$$x = train\_ambg\_lfm(taup, n, pri, bw)$$

where

Symbol	Description	Units	Status
taup	*pulse width*	*seconds*	*input*
n	*number of pulses in train*	*none*	*input*
pri	*pulse repetition interval*	*seconds*	*input*
bw	*the LFM bandwidth*	*Hz*	*input*
x	*array of bimodality function*	*none*	*output*

Note this function will generate identical results to the function *"train_ambg.m"* when the value of *bw* is set to zero. In this case, Eq. (4.43) and (4.35) are identical.

MATLAB Function** "train_ambg_lfm.m" **Listing

```
function x = train_ambg_lfm(taup, n, pri, bw)
% This code was developed by Stephen Robinson, a senior radar engineer at
% deciBel Research in Hunstville AL
if (taup >= pri/2)
   'ERROR. Pulse width must be less than the PRI/2.'
   return
end
eps = 1.0e-6;
q = -(n-1):1:n-1;
offset = 0:0.0533:pri;
[Q, S] = meshgrid(q, offset);
Q = reshape(Q, 1, length(q)*length(offset));
S = reshape(S, 1, length(q)*length(offset));
tau = (-taup * ones(1,length(S))) + S;
fd = -bw:0.033:bw;
[T, F] = meshgrid(tau, fd);
Q = repmat(Q, length(fd), 1);
S = repmat(S, length(fd), 1);
N = n * ones(size(T));
val1 = 1.0-(abs(T))/taup;
val2 = pi*taup*(F+T*(bw/taup)).*val1;
val3 = abs(val1.*sin(val2+eps)./(val2+eps));
val4 = abs(sin(pi*F.*(N-abs(Q))*pri+eps)./sin(pi*F*pri+eps));
x = val3.*val4./N;
[rows, cols] = size(x);
x = reshape(x, 1, rows*cols);
T = reshape(T, 1, rows*cols);
indx = find(abs(T) > taup);
x(indx) = 0.0;
x = reshape(x, rows, cols);
return
```

Problems

5.1. Derive Eq. (5.47).

5.2. Show that Eq. (5.79) and Eq. (5.80) are equivalent.

5.3. Derive an expression for the ambiguity function of a Gaussian pulse defined by

$$x(t) = \frac{1}{\sqrt{\sigma}\ \sqrt[1/4]{\pi}} \exp\left[\frac{-t^2}{2\sigma^2}\right] \qquad ;0 < t < T$$

where T is the pulsewidth and σ is a constant.

5.4. Write a MATLAB code to plot the 3-D and the contour plots for the results in Problem 5.3.

5.5. Derive an expression for the ambiguity function of a V-LFM waveform, illustrated in figure below. In this case, the overall complex envelope is

$$\tilde{x}(t) = \tilde{x}_1(t) + \tilde{x}_2(t) \qquad ;-(T < t < T)$$

where

$$\tilde{x}_1(t) = \frac{1}{\sqrt{2T}} \exp[-\mu t^2] \qquad ;-T < t < 0$$

and

$$\tilde{x}_2(t) = \frac{1}{\sqrt{2T}} \exp[\mu t^2] \qquad ;0 < t < T$$

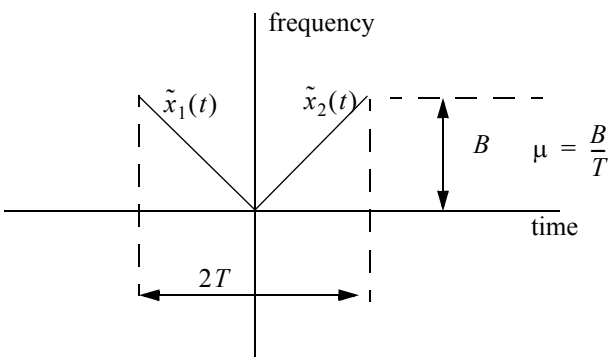

5.6. Using the stationary phase concept, find the instantaneous frequency for the waveform whose envelope and complex spectrum are, respectively, given by

$$r(t) = \frac{1}{\sqrt{T}} \exp\left[-\left(\frac{2t}{T}\right)^2\right] \qquad ;0 < t < T$$

and

$$|X(f)| = \frac{1}{\sqrt{B}} \exp\left[-\left(\frac{2f}{B}\right)^2\right]$$

5.7. Using the stationary phase concept find the instantaneous frequency for the waveform whose envelope and complex spectrum are respectively given by

$$r(t) = \frac{1}{\sqrt{\tau_0}} Rect\left(\frac{t}{\tau_0}\right) \quad ; \ 0 < t < \tau_0$$

and

$$|X(\omega)| = \frac{2}{\sqrt{B}} \frac{1}{\sqrt{1 + (2\omega / B)^2}}$$

5.8. Write detailed MATLAB code to compute the ambiguity function for an NLFM waveform. Your code must be able to produce 3-D and contour plots of the resulting ambiguity function. Hint: Use Eq. (5.90).

5.9. Revisit the analyses performed in Chapter 2 for the effective bandwidth and effective duration of the LFM waveform. Write a short discussion to outline how do the range and Doppler resolution are different from the theoretical limits used in this chapter.

5.10. Write a detailed MATLAB code to compute the ambiguity function for an SFW waveform. Your code must be able to produce 3-D and contour plots of the resulting ambiguity function. Hint: use Eq. (5.43).

5.11. Prove that cuts in the ambiguity function are always defined by an ellipse. Hint: Approximate the ambiguity function using a Taylor series expansion about the values $(\tau, f_d) = (0, 0)$; use only the first three terms in the Taylor series expansion.

5.12. The radar uncertainty principle establishes a lower bound for the time bandwidth product. More specifically, if the radar effective duration is τ_e and its effective bandwidth is B_e; show that $B_e^2 \tau_e^2 - \rho_{RDC}^2 \geq \pi^2$, where ρ_{RDC} is the range-Doppler coupling coefficient defined in Chapter 4. Hint: Assume a signal $x(t)$, write down the definition of ρ_{RDC}, and use Shwarz inequality on the integral

$$(-j2\pi) \int_{-\infty}^{\infty} t x^*(t) x'(t) dt .$$